Research Article | Vol. 15, No. 9 / 1 Sep 2024 / Biomedical Optics Express 5115

Biomedical Optics EXPRESS

Longitudinal tracking of perfluorooctanoic acid exposure on mammary epithelial cell spheroids by dynamic optical coherence tomography

LIN YANG,[1] PAN JI,[1] ABEL A. MIRANDA BUZETTA,[2,3] HAOLIN LI,[4] MATTHEW R. LOCKETT,[2,5] HAIBO ZHOU,[4] AND AMY L. OLDENBURG[1,5,6,*]

[1]*Department of Physics and Astronomy, The University of North Carolina-Chapel Hill, Chapel Hill, NC 27599, USA*
[2]*Department of Chemistry, The University of North Carolina-Chapel Hill, Chapel Hill, NC 27599, USA*
[3]*School of Medicine, The University of North Carolina-Chapel Hill, Chapel Hill, NC 27599, USA*
[4]*Department of Biostatistics, The University of North Carolina-Chapel Hill, Chapel Hill, NC 27599, USA*
[5]*Lineberger Comprehensive Cancer Center, The University of North Carolina-Chapel Hill, Chapel Hill, NC 27599, USA*
[6]*Biomedical Research Imaging Center, The University of North Carolina-Chapel Hill, Chapel Hill, NC 27599, USA*
[*]*aold@physics.unc.edu*

Abstract: We investigated the morphology and intracellular motility of mammary epithelial cell (MCF10DCIS.com) spheroids cultured in 3D artificial extracellular matrix under perfluorooctanoic acid (PFOA) exposure. Dynamic optical coherence tomography (OCT) was employed for real-time, non-invasive imaging of these spheroids longitudinally over 12 days under PFOA exposures up to 500 μM. Despite no significant changes in volume or asphericity of spheroids, morphological alterations were observed in OCT images of spheroids at 100 μM on Day 12 and from Day 4 at 500 μM. Intracellular motility was assessed by the inverse-power-law exponent of the speckle fluctuation spectrum (α), and an autocorrelation-based motility amplitude (M). Linear regression indicated that both PFOA concentration and culture time are highly significant predictors for both α and M ($p < 0.001$ for all). Both PFOA concentration and culture time have positive associations with α and negative association with M, where increased α indicates suppression of higher frequency fluctuations ($\sim> 2$ Hz) relative to those at lower frequencies, and decreased M indicates overall suppression of intracellular motility. This study can lead to the future development of biomarkers for per- and polyfluoroalkyl substances (PFAS) exposure using dynamic OCT and its associated toolkit of quantitative metrics.

1. Introduction

Per- and polyfluoroalkyl substances (PFAS), such as perfluorooctanoic acid (PFOA), are synthetic fluorinated molecules extensively used in industry and consumer products, persisting in the environment and bioaccumulating in human serum and breast milk [1]. PFOA is implicated in an increased incidence of breast cancers, impacting tumorigenesis in mammary epithelial cell (MEC) lines by dysregulating metabolism, accelerating cell proliferation, and promoting cell migration and invasion through mechanisms involving peroxisome proliferator-activated receptor α (PPARα) or estrogen receptor activation [2–4]. However, current research relies on two-dimensional (2D) monolayer cell models. Three-dimensional (3D) models, such as spheroids, display distinct responses to environmental toxins like PFAS, as 3D models more accurately recapitulate *in vivo* tissue architecture, and mimic physiologically relevant interactions and toxicant responses observed *in vivo* [5–7]. Furthermore, 3D spheroid models better capture

#530775 https://doi.org/10.1364/BOE.530775
Journal © 2024 Received 21 May 2024; revised 30 Jul 2024; accepted 30 Jul 2024; published 8 Aug 2024

Biomedical Optics EXPRESS

microenvironmental factors, such as hypoxia, paracrine cell signaling, matrix interactions, and chemical gradients, that influence cell motility — an important cellular function underlying the migration, invasion, and metastasis of breast cancer, which might be associated with responses induced by environmental toxicants [7,8]. However, current methods for assessing 3D spheroids often require cell fixation and staining [9], which precludes efficient longitudinal analysis for capturing time-dependent exposure responses. This poses challenges for studying environmental toxicants like PFAS with long induction times for processes such as tumorigenesis in breast epithelial cell lines [10].

To address these challenges, Optical Coherence Tomography (OCT) offers depth-resolved imaging using near-infrared light scattering, analogous to ultrasound imaging, with micrometer-scale resolution, millimeter-scale penetration depth, and real-time imaging speed [11]. OCT is non-invasive and can uniquely capture the entire morphology and intracellular dynamics of spheroids cultured in 3D extracellular matrix (ECM) longitudinally. Previously, we employed OCT to monitor growth of MEC spheroids over weeks, and quantified morphological changes (including size, lumen size, and asphericity) under culture conditions that modified stromal-epithelial interactions [12].

As an interferometric technique, OCT is phase-sensitive and thus exhibits fluctuations from sub-wavelength (nanoscale) motions of light scattering structures. This makes OCT particularly suitable for detecting "intracellular motility," *i.e.,* in-place motions of subcellular components (such as organelle transport and membrane undulations) that occur on the nanoscale within short (seconds to minutes) time scales, reflecting movements related to cell state, metabolic processes, and other cellular activities [13,14]. Since intracellular motility was initially detected by holographic optical coherence imaging [15], researchers have developed a technique called dynamic OCT (D-OCT), which uses speckle fluctuation statistics to distinguish live MEC spheroids from surrounding ECM [16]. Recently, D-OCT has been extensively used to observe cellular dynamics and viability in response to a variety of stimuli. Observations include increased ciliary beat frequency of airway epithelial tissues under ATP-γ-S stimulation [17], activity suppression in hepatocytes by glycolysis inhibitors [18], metabolic and necrotic activities of mammary tumor spheroids [19] and tracking invasions of breast cancer cells [20].

In this study we utilize two previously established metrics extracted from OCT images to quantify the intracellular motility of MEC spheroids: the inverse-power-law exponent of the speckle fluctuation spectrum (α), and an autocorrelation-based motility amplitude (M). Importantly, both α and M are independent of light attenuation and sensitivity roll-off within the image, making them suitable for 3D spheroid imaging. Previously, both α and M exhibited significant differences in 3D MEC-fibroblast co-cultures as a function of modifications to stromal-epithelial cell interactions [21]. Additionally, α and M were employed in a high-throughput approach to assess responses of 3D MEC spheroid models to toxicant exposure, with findings validated by a standard MTT assay [22]. Moreover, dynamic OCT revealed time- and concentration-dependent responses and cell line-specific response patterns to a microtubule stabilizer (Paclitaxel, Taxol) and a myosin II inhibitor (Blebbistatin) via different motility suppression mechanisms [23]. This study aims to investigate the effects of PFOA exposure on a pre-malignant breast cell line – MCF10DCIS.com – cultured in spheroids while using D-OCT to establish candidate biomarkers of risk associated with PFOA exposure. The MCF10DCIS.com model is particularly suited for this research as it closely mimics the early stages of breast cancer development, making it favorable for screening PFAS molecules and studying the mechanisms of environmental toxicant exposures [24].

Biomedical Optics EXPRESS

2. Materials and methods

2.1. Cell lines and reagents

Premalignant, basal-like MCF10DCIS.com cells were obtained from Karmanos Cancer Institute (Detroit, MI, USA) and were cultured in Dulbecco's modified Eagle's medium (DMEM)/F12 nutrient mixture supplemented with 5% horse serum, 10 µg/mL insulin, 20 ng/mL Epidermal Growth Factor (GIBCO, Thermo Fisher Scientific, Waltham, MA, USA), 0.5 µg/mL hydrocortisone (Sigma-Aldrich, St. Louis, MO, USA), 0.1 µg/mL cholera toxin (MilliporeSigma, Burlington, MA, USA) and 1% penicillin-streptomycin. All cells were maintained as monolayers in a humidified incubator at 37°C with 5% CO_2. The PFOA compound used for spheroid culture exposures in this study was purchased from Sigma-Aldrich.

2.2. 3D culture and PFOA exposure

The 3D cultures used in this study were constructed following the methods previously described [22,23]. Briefly, after reached 70% confluency in 2D cultures, cells were seeded at a constant density of 30,000 cells/cm^3 into 60 µL of a biologically derived ECM comprised of a 1:1 ratio of collagen I (rat tail) to Matrigel (Fisher Scientific, Hampton, NH) [25]. The final collagen concentration was 1 mg/mL. The cell-laden gels were then plated into individual wells of 96-well cell culture plates (diameter: 6 mm). After gelation, 200 µl of the culture medium was added to each well and refreshed every 2-3 days. To allow for spheroid formation and growth, MCF10DCIS.com cells were cultured in 3D for 10 days before PFOA exposure. The cultures were then exposed to PFOA daily for up to 12 days (0 µM, 0.01 µM, 1 µM, 10 µM, 30 µM, 100 µM or 500 µM). These concentrations were chosen based on reported levels found in human serum and breast milk samples, which vary from 0.01 µM to nearly 25 µM among individuals living or working in highly contaminated areas [26]. Note that the utilization of higher concentrations than those observed *in vivo* aimed to examine the effects of PFOA over a condensed exposure period. By employing higher concentrations than those typically observed *in vivo*, we sought to reflect the specific experimental conditions of prolonged exposure over a short period after spheroid formation. Dynamic OCT imaging of PFOA-exposed cultures was performed prior to exposure ("Day 0"), and then at Day 1, Day 4, Day 8, and Day 12 after the initial exposure. Three independent cultures per condition (*i.e.*, concentration of PFOA) were prepared and tracked longitudinally with dynamic OCT. An average of 33 spheroids per culture over the 3 independent replicates (*i.e.,* $n = 98$ per condition) were imaged by dynamic OCT. The images were segmented into regions of interest (ROIs) using a custom semi-automated MATLAB script, resulting in a total of $n = 60$-200 ROIs measured at each concentration and time point.

2.3. Dynamic OCT imaging and extraction of metrics

The system used for dynamic OCT imaging of the 3D cultures was a commercial, spectral-domain optical coherence tomography (SD-OCT) system (GAN621, Thorlabs, Newton, NJ), with the system layout shown in Fig. 1(A). Briefly, the system is composed of three main components: the light source, a Michelson interferometer, and a spectrometer. A superluminescent diode (SLD) source was used as the light source, with a central wavelength of 890 nm and bandwidth of 142 nm. The light from the SLD was split into reference and sample arms in the Michelson interferometer. The sample light, with a power of ~1 mW, focused on the sample by an 18 mm focal length objective lens (LSM02-BB, Thorlabs, Newton, NJ). The backscattered sample light was combined with the reference light and then directed to the spectrometer, where spectral interferograms were captured by a line-scan CCD camera with 2048-pixel and operated at an A-line rate of 50 kHz for this study. The resolution of the OCT system was ~5 µm × 2.8 µm ($x \times z$) in aqueous medium, and the signal-to-noise ratio (SNR) was ~96 dB. B-scans were performed on the samples over 5 mm × 1.48 mm in $x \times z$ (in aqueous medium), generating

Biomedical Optics EXPRESS

B-mode (cross-sectional) image frames of 1000 × 1024 pixels. 208 frames per time series were captured at 10 Hz at each lateral (y) position to capture cellular dynamics. For 3D morphology analysis, a total of 200 lateral positions over 2 mm (with a step size of 10 μm) were imaged per well to capture as many spheroids as possible, while a total of 32 lateral positions over 0.96 mm (with a step size of 30 μm) were imaged per well for intracellular motility analysis. Note that while the same culture wells were scanned over time, we did not co-register individual spheroids between time points. Instead, we relied on sampling a representative population of spheroids within each well.

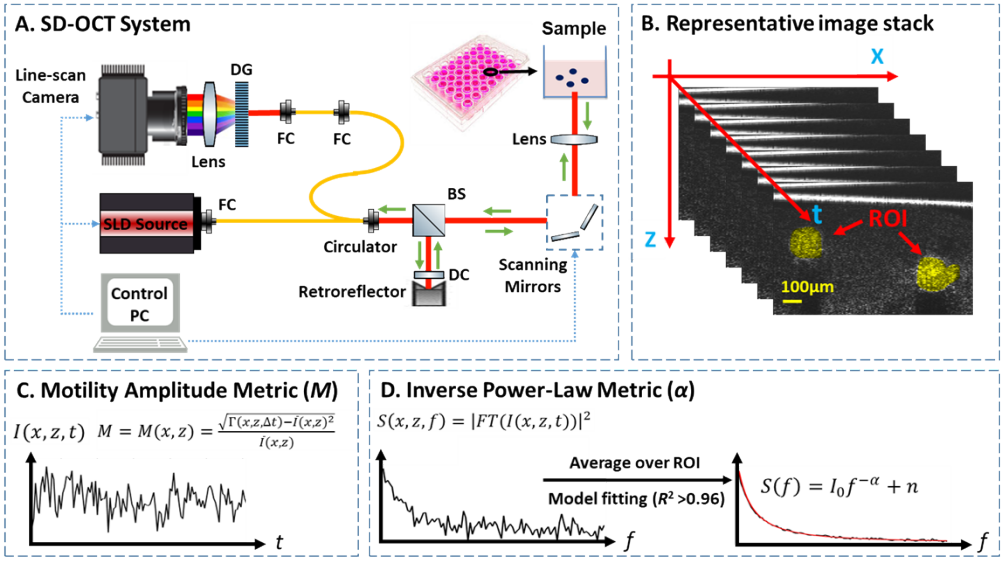

Fig. 1. Overview of OCT hardware, data collection, and analysis pipeline for spheroids maintained in a 96-well plate. (A) Spectral domain OCT system; FC: fiber coupler; BS: beam splitter; DG: diffraction grating, DC: dispersion compensation glass; (B) a representative time-stack of 208 successive B-mode images for analysis; ROI: region of interest; (C) metric for motility amplitude; (D) power spectral analysis of OCT fluctuations. FT: Fourier transform.

All image analyses were conducted as described in our previous studies [12,21–23]. Briefly, depth-resolved OCT images were derived from raw spectral images where the intensity at each image pixel, $I(x, z)$, was calculated from the absolute value of the complex analytic signal, which is obtained by Fourier transform of the spectral domain OCT data following reference subtraction and digital dispersion compensation [21]. For 3D morphology analysis, spheroids were initially identified and segmented by custom semi-automated MATLAB scripts. The volume and asphericity of each spheroid were then extracted as described previously [12]. Asphericity is calculated as the ratio of the volume of a perfect sphere with the same surface area as the spheroid, to the actual volume of the spheroid. A value of 1 indicates a perfect sphere, with higher values indicating more irregular shapes. For intracellular motility analysis, a representative time series of cross-sectional OCT images of MEC spheroids, as shown in Fig. 1(B), was utilized to generate movies for analysis of the dynamics. Each spheroid, consisting of hundreds to thousands of cells, was segmented as a single region of interest (ROI) using custom semi-automated MATLAB scripts; a representative ROI is color-coded in yellow in Fig. 1(B). The semi-automated approach for masking spheroids is as follows. For each time series, a time-averaged OCT image is generated upon which a user draws a mask containing only ECM surrounding the spheroids. The intensity within this ECM mask is then used to define a depth-dependent intensity threshold as twice

Biomedical Optics EXPRESS

the mean ECM intensity within each row, to account for sensitivity variation with depth. The threshold is applied to identify spheroids (defined as contiguous regions > 800 pixels in size and lying above row 650), which also excluded holes with low scattering intensity from the analysis. A small number of spheroids were missed by this method and were segmented by hand.

The temporal fluctuation of speckle intensity at each pixel, $I(x, z, t)$, as depicted in Fig. 1(C), results from the movements of intracellular particles that backscatter OCT light. These speckle fluctuations were extracted from the time series and characterized by two parameters: the "motility amplitude"(M), which quantifies the modulation amplitude of the speckle fluctuations over time, and the power-law exponent (α), which describes the decay of the power spectral density with frequency, as illustrated in Fig. 1(D). M is an autocorrelation-based modified standard deviation normalized by average pixel intensity [21], offering two complementary advantages for dynamic OCT data analysis: the temporal autocorrelation obtained at the sampling time Δt, $\Gamma(x, z, \Delta t)$, inherently omits shot noise that decorrelates instantaneously, while normalization by temporally averaged pixel intensity eliminates the depth-dependent SNR roll-off, making M intensity- and depth-invariant for deep tissue imaging. M at each pixel was then averaged spatially across each ROI to measure the overall M of a spheroid, representing the overall amplitude of the in-place motions within the spheroid. Additionally, the frequency (f) dependence of the motility signals, as illustrated in Fig. 1(D), was analyzed by computing the power spectral density $S(x, z, f)$ from the discrete Fourier transform of the time signal $I(x, z, t)$ at each pixel, where the spectra were then spatially averaged over each ROI and fitted to an inverse power-law model with the power exponent α [21].

For each ROI spectrum, a goodness-of-fit test was conducted for model fitting to ensure that only data with $R^2 > 0.96$ compared to the model were considered in further analysis. α serves as a metric that measures the decay rate of the speckle fluctuations arising from intracellular motion with frequency, where lower values of α correspond to a relatively larger amount of high frequencies (typically frequencies > 2 Hz), which correspond to either more rapid and/or more rapidly vibrating motions. Together, the two metrics α and M are employed as independent metrics to analyze the intracellular motility of each spheroid (one ROI), with an average of 98 spheroids analyzed at each culture condition (concentration and time). To assess the time- and concentration-dependence of intracellular motility, linear regression using R (v. 4.4.0) was performed to model α and M as a function of time, concentration, and a time-concentration interaction term.

3. Results and discussion

3.1. OCT reveals morphological alterations in MEC spheroids under PFOA exposure

OCT-based measurements of volume and asphericity of the MCF10DCIS.com spheroids are shown in Fig. S1. Significant increases in volume and asphericity were observed for some concentrations over 12 days post-exposure, which we attribute to normal growth of spheroids. However, no significant changes were observed relative to the 0 µM concentration controls based on multiple comparison t-tests with Bonferroni correction, indicating that the size and external shape of the spheroids remain relatively stable across exposure to different PFOA concentrations.

Despite this negative finding, we did observe internal structural alterations in OCT images of the spheroids, as illustrated in Fig. 2. Representative images depict the time-averaged signal intensity from 208 consecutive images per time series for each condition, with the background representing the ECM and round-shaped areas of high intensity indicating the presence of spheroids. Horizontal lines appearing in some images correspond to artifacts from the top and bottom surfaces of the glass plate underneath the cell culture.

As depicted in Fig. 2 and S2, despite an increase in spheroid volume over time attributed to normal growth, (noting that these images only show one cross-section), no noticeable morphological changes were observed inside the spheroids in the control group or for concentrations below 100

Biomedical Optics EXPRESS

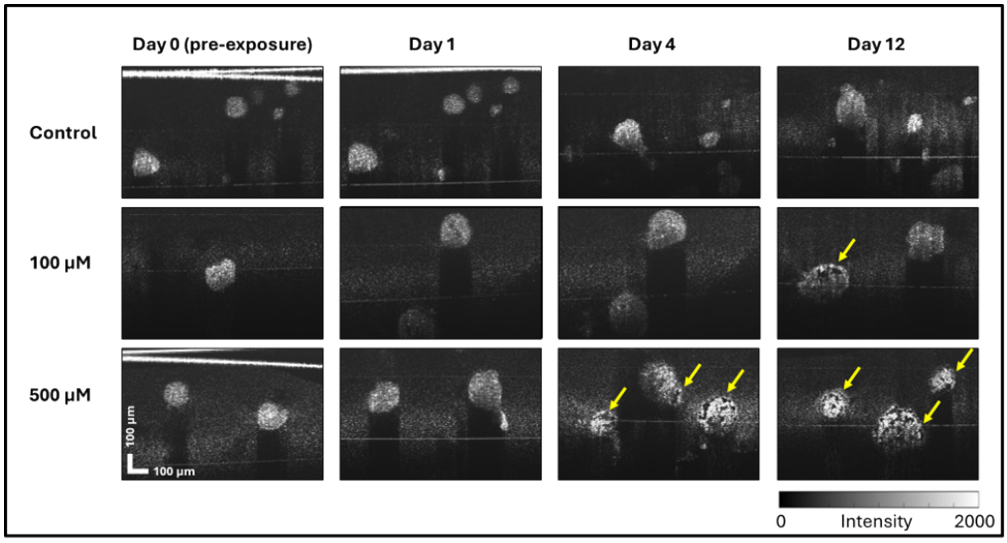

Fig. 2. Representative time-averaged OCT images of MCF10DCIS.com spheroids treated with different concentrations of PFOA for up to 12 days. Arrows indicate regions of low light scattering (apparent holes) observed inside the spheroids.

µM of PFOA throughout the entire 12-day period. Furthermore, no morphological changes were observed for the 100 µM concentration until Day 12, at which time some regions of low intensity, indicated with yellow arrows, suggest the appearance of holes within the spheroids. Holes also began to appear in the MEC spheroids at an earlier time point (Day 4) of higher exposure to 500 µM PFOA, with a notably higher hole density than observed on Day 12. The multiple holes we identified in the spheroids are small, approximately 20 µm in diameter, and scattered, which are different from the centrally located, single lumens that typically form in MEC spheroids and indicate healthy cell polarization. The irregularly distributed holes observed here suggest regions of cell death induced by the high concentration of PFOA, which is similar to previous findings by Pierozan *et al.* In their study using MCF10A cells in 2D cultures, both the cell viability (MTT assay) and number of cells (DAPI staining) were significantly reduced at concentrations of 250 µM and above for 24-72 hours post-exposure [3].

3.2. *Dynamic OCT visually reveals decreases of M in MEC spheroids under PFOA exposure*

Representative images of motility amplitude (M) of MCF10DCIS.com spheroids at varying culture times and PFOA concentrations are illustrated in Fig. 3 and S3. M signals were computed at each pixel from the corresponding 208 consecutive OCT images per time series for each condition shown in Fig. 2. The background in the images represents the low motility amplitude of ECM, while round-shaped areas indicate the high motility amplitudes of the spheroids shown in Fig. 2, respectively, labeled with M averaged over corresponding spheroids.

As depicted in Fig. 3 and S3, no noticeable differences in M were observed for 0.01 µM - 30 µM concentrations of PFOA exposure throughout the entire 12-day period, when compared to their 0 µM control counterpart at the same culture time point. For higher concentrations of 100 µM and 500 µM shown in Fig. 3, no noticeable differences in M were observed on Day 0 (pre-exposure) and Day 1. On Day 4, M was only 0.09 for 500 µM PFOA exposure, compared to 0.31 at 0 µM, indicative of suppression of intracellular dynamics under such high concentration

Biomedical Optics EXPRESS

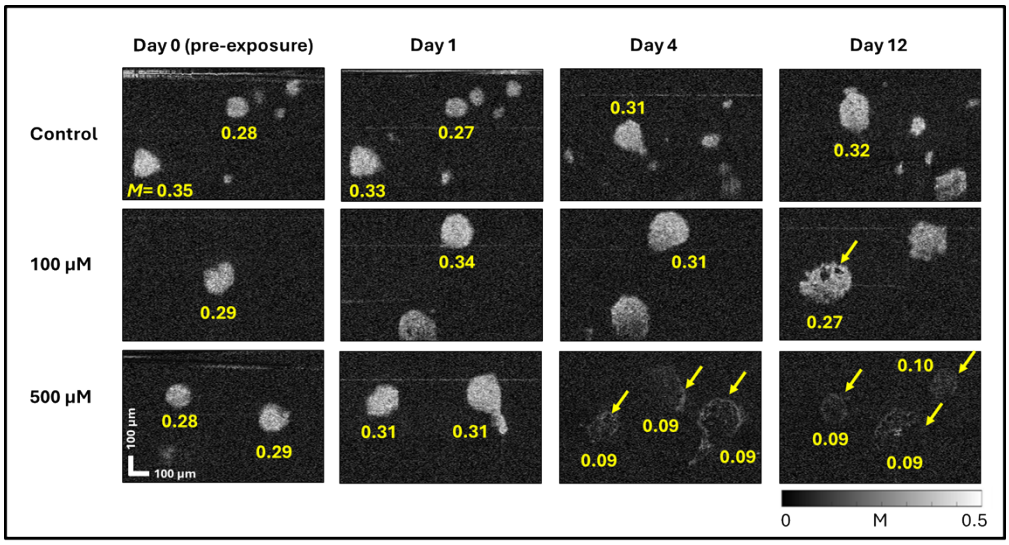

Fig. 3. Representative images of M derived from D-OCT images of MCF10DCIS.com spheroids treated with different concentrations of PFOA for up to 12 days.

PFOA exposure. On Day 12, compared to the 0 µM control, M of the spheroid was only 0.27 for 100 µM and remained at around 0.09 for 500 µM PFOA.

As described in the methods, an intensity threshold was applied during the generation of ROIs to exclude regions or holes with low scattering intensity from the analysis. Therefore, all values of M were computed exclusively from the high light scattering regions, ensuring that potentially low values of M in the holes did not influence the analysis of the entire spheroid.

Figure 4 presents time-averaged OCT images (a), motility images (b), and overlays of motility (M) represented in a hot colormap onto grayscale time-averaged OCT images (c) for both the control condition and exposure to 500 µM PFOA at Day 12 post-exposure. Note that in panel (c), only M within the segmented ROIs is overlaid on the time-averaged images. In panels (b) and (c), a decrease in spheroid motility with PFOA exposure is visually evident, with the average motility decreasing from 0.27 for the control to 0.11 for 500 µM. Visualization 1 in the supplemental materials display the D-OCT images of the control and 500 µM (the time-averages of which are shown in panels (a)), respectively, showcasing 208 frames of the image stacks at 4x real-time (40 Hz frame rate).

3.3. *Dynamic OCT quantifies the time- and concentration-dependent responses of MEC spheroids to PFOA exposure*

Figure 5(a) and (b) shows the PFOA concentration-dependent changes in M and α of MCF10DCIS.com spheroids at each culture time. Here we hypothesized that M and α of MEC spheroids would exhibit concentration-dependent changes in the 3D culture at longer culture times, similar to what we previously observed in the 3D MEC model system in response to various toxicants [22,23]. To assess the PFAS concentration-dependence of intracellular motility, multiple comparison t-tests with Bonferroni correction were performed to compare α and M at each concentration against their corresponding 0 µM controls at each culture time. P-values were calculated to indicate statistically significant differences, where the critical p-value was set to 0.007 after Bonferroni correction. In addition, one-way ANOVA analysis was used to conduct overall comparisons among concentration levels for given time points.

Biomedical Optics EXPRESS

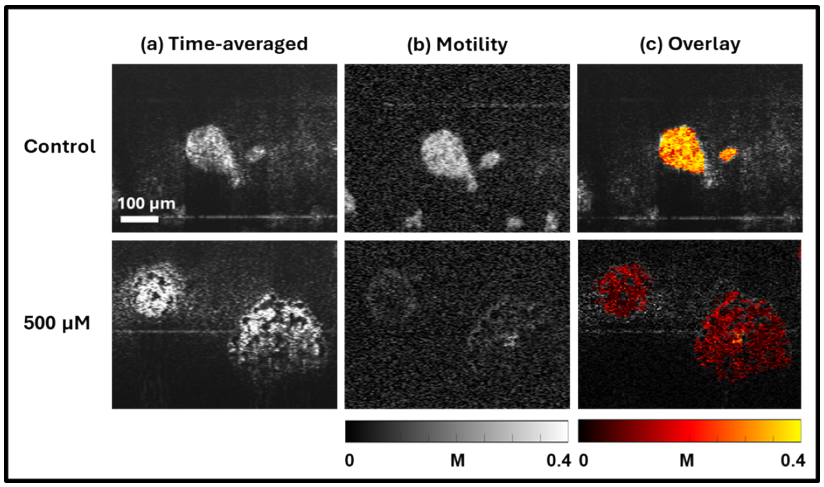

Fig. 4. Representative time-averaged OCT (a) motility amplitude (M) images (b), and the overlay of M (hot color, within ROIs) onto grayscale time-averaged OCT images (c) for the control and 500 µM samples at Day 12 post-exposure. See Visualization 1 corresponding to the control and 500 µM OCT image datasets depicted here, which display 208 frames of the OCT image stack in 4x real-time.

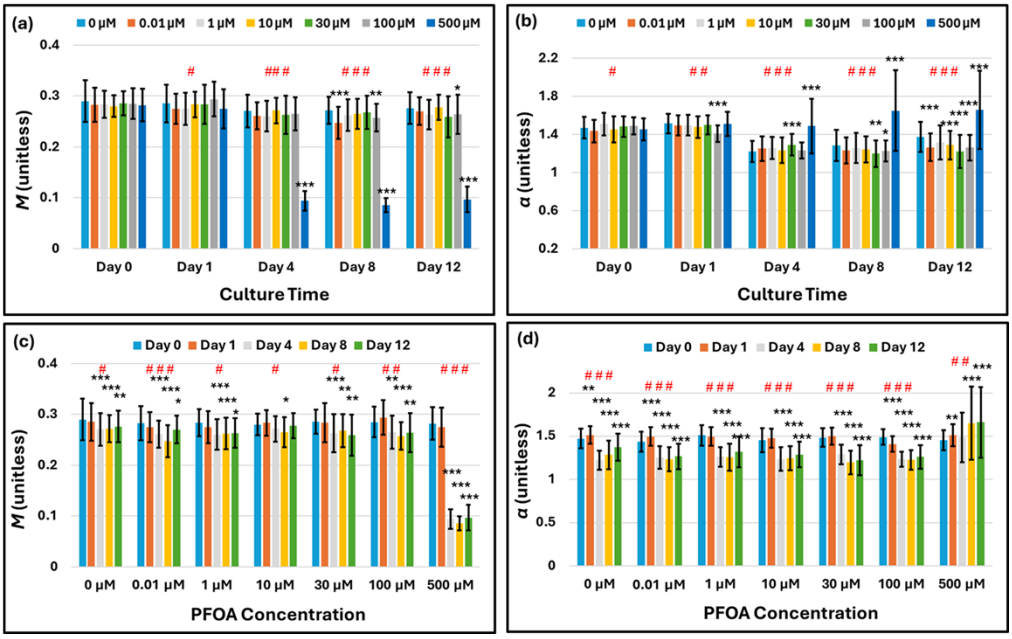

Fig. 5. Time- and PFOA concentration-dependent M and α of MCF10DCIS.com spheroids with average of $n = 98$ per condition. Critical p-values for (a) and (b): $^{*}p < 0.007$, $^{**}p < 0.0007$, $^{***}p < 0.00007$ relative to the 0 µM control within each culture time group. Critical p-values for (c) and (d): $^{*}p < 0.01$, $^{**}p < 0.001$, $^{***}p < 0.0001$ relative to the Day 0 control within each concentration group. Critical p-values for one-way ANOVA analysis: $^{\#}p < 0.05$, $^{\#\#}p < 5\times10^{-8}$, $^{\#\#\#}p < 5\times10^{-16}$. Error bars represent mean ± STD.

Biomedical Optics EXPRESS

From Fig. 5(a), no significant concentration-dependent changes in M were observed for concentrations below 100 μM over the 12-day exposure period, except a significant decrease in M at 0.01 μM ($p < 0.00007$) on Day 8 compared to the 0 μM control. This significant decrease is likely due to natural variation, which is similar to the natural variation observed in previous publications [22,23]. Furthermore, exposure to 100 μM PFOA resulted in significant decreases in M on Day 8 ($p < 0.0007$) and Day 12 ($p < 0.007$), with the distributions of M shown in Fig.S4. Importantly, exposure to 500 μM PFOA consistently resulted in pronounced decreases in M starting from Day 4 through Day 12 ($p < 0.00007$ for all). The analysis results from ANOVA follow the same trend as the t-tests. Specifically, the time points with more significant results from pairwise t-tests are more likely to have smaller p-values from the ANOVA.

As shown in Fig. 5(b), compared to M, trends in α are similar but relatively more complicated (noting that an increase in α is often associated with a decrease in M when cell death is implicated, as discussed below). On Day 0 and 1, no significant concentration-dependent changes in α were observed for all concentrations except a significant decrease of 100 μM ($p < 0.00007$) on Day 1. From Day 4 to Day 12, significant variations of α were observed for some concentrations below 500 μM. Specifically, on Day 4, 30 μM exhibited significantly increased α while on Day 8, both 30 μM and 100 μM showed significant decrease in α. On Day 12, all concentrations below 500 μM exhibited significant decreases in α except 1 μM. However, despite the mixed responses for lower concentrations, 500 μM exhibited significant increases in α consistently from Day 4 to Day 12 compared to the 0 μM controls.

Figure 5(c) and (d) shows the culture time-dependent changes in M and α of MCF10DCIS.com spheroids at each PFOA concentration. Similarly, multiple comparison t-tests with Bonferroni correction were performed to compare α and M at each time point against their corresponding Day 0 controls at PFOA concentration. P-values were calculated to indicate statistically significant differences, where the critical p-value was set to 0.01 after Bonferroni correction. Notably, M and α values for all concentrations lower than 500 μM show significant variations over time, as illustrated in Fig. 5(c) and (d), especially significant decreases (compared to Day 0) starting on Day 4, which might be associated to developmental changes of the MEC spheroids over culture time or biological variability in cell growth, which have been previously observed in MCF10DCIS.com spheroids [22]. However, no significant changes of both α and M between concentrations were found on the pre-exposure controls on Day 0, as illustrated in Fig. 5(a) and (b), suggesting α and M are stable metrics for spheroids within the same stage of their growth cycle. Similar to Fig. 5(a), the analysis results from the one-way ANOVA for overall comparison among time points for given concentration levels follow the same trend as the t-tests in (c), and (d). The details of all analysis results from the ANOVA are presented in the Supplementary Materials.

The diverse responses in intracellular motility, especially α, imply potentially complex interactions between culture time and PFOA concentration levels. Utilizing the extensive dataset obtained from our measurements (average of $n = 98$ per condition), we explored the association of M and α on culture time, PFOA concentration, and an additional interaction term between these variables. Due to the skewness of PFOA concentration and potential nonlinear relationship, we define the "low concentration level" as any concentrations ≤ 100 μM, and "high concentration level" as the concentration level of 500 μM. In addition, due to the observed nonlinear time effect in Fig. 5, we define the "short culture time" as days 0 and 1, and "long culture time" as days 4, 8, and 12. Then we fit the following linear regression model in R (v. 4.4.0):

$$(\alpha,\ M) = \beta_0 + \beta_1 t + \beta_2 C + \beta_3 tC \tag{1}$$

where t is the indicator of short culture time, C is the indicator of low PFOA concentration level, and β_i are the regression coefficients for which estimates are summarized in Table 1. This linear

Biomedical Optics EXPRESS

regression model is designed to interpret the time effects for both concentration levels, as well as the concentration effects between the short and long time points.

Table 1. Parameter Estimates for Motility Metrics[a]

Parameters		α	M
Intercept	β_0	1.581 (0.010) * * *	0.092 (0.002) ***
Culture Time Effect	β_1	-0.099 (0.015) * * *	0.179 (0.003) ***
PFOA Concentration Effect	β_2	-0.316 (0.010) * * *	0.174 (0.002) ***
Culture Time and Concentration Interaction Effect	β_3	0.312 (0.016) * * *	-0.161 (0.003) ***

[a]Estimate (standard error) obtained using linear regression according to Eq. (1).
[a]Note: Significance levels: ***, $p < 0.001$; **, $p < 0.01$; *, $p < 0.05$.
[a]Multiple R^2 for α and M are 0.334 and 0.729, respectively.

The results indicate that the culture time strongly predicts both α and M (p<0.001 for both). For high PFOA concentration level, α and M during the short culture time are 0.099 lower and 0.179 higher compared to those during the long culture time, respectively, suggesting slight suppression of lower frequency fluctuations or promotion of higher frequency fluctuations and suppression of the overall motility amplitude over time. PFOA concentration is also a significant predictor for both α and M ($p < 0.001$ for both). In particular, for long culture time, α and M for low PFOA concentration are 0.316 lower and 0.174 higher compared to those for high PFOA concentration, indicating selective suppression of higher frequency fluctuations and suppression of the overall motility amplitude over increasing concentration. The interaction term is also significant ($p < 0.001$ for both), suggesting a complex interplay among PFOA concentration, culture duration, and intracellular dynamics. The multiple R^2 values for α and M are 0.334 and 0.729, respectively, indicating a limitation of the current model due to the absence of measurements between 1 and 4 days of culture time and between 100 µM and 500 µM of PFOA concentration levels. Future work is needed to investigate more precise time points and concentration levels at which substantial changes take place. Nonetheless, this model captures the overall trends of the effects of PFOA concentration and culture time on α and M.

The trends found in the above linear regression are consistent with a specific pattern of suppression on intracellular motility observed in a previous live/fixed analysis on MCF10DCIS.com spheroids [22]. Specifically, Yu *et al.* reported a significant increase in α and a significant decrease in M values between live and formalin-fixed cells ($p < 0.0001$). In a separate study involving Doxorubicin exposure, Yu *et al.* found that this specific response pattern, *i.e.*, increased α and decreased M, was correlated with cell death, as validated by MTT assay. Notably, the appearance of holes in the spheroids coincided with lower M and higher α, suggesting a potential correlation between structural alterations and loss of cellular viability. Further studies are needed to elucidate the mechanistic links between structural changes and M/α alterations.

As expected, dynamic OCT revealed time- and concentration-dependent responses of MCF10DCIS.com spheroids exposed to PFOA, a compound that is known to affect cell proliferation and potentially induce cell death of MEC cell lines [3,27]. In particular, the data suggests that high concentration PFOA exposures may result in suppression of intracellular motility within as short a period as a few days. Since the utilization of higher concentrations than those observed *in vivo* aimed to examine the effects of PFOA over a condensed exposure period, the observed rapid onset of cellular changes suggests a potential for significant risks of cell death over time.

As previously discussed, the specific pattern of suppression on intracellular motility (increased α and decreased M) observed in this study may be attributed to reduced cell viability for breast epithelial cell lines exposed to PFOA, consistent with a report by Pierozan *et al.* The suppression pattern is particularly evident at concentrations at or above 250 µM and as early

Biomedical Optics EXPRESS

as 24 hours post-exposure. Reduced cell viability in PFOA-exposed MEC has been linked to PFOA-induced PPARα-dependent changes in proliferation, metabolism, and dysregulation in cell-cycle progression, which suggest potential tumor development and progression [3]. Other research findings point to alternative pathways, such as the p53/mitochondrial pathway and tumor necrosis factor-α/nuclear factor κB (TNF-α/NF-κB), which are more relevant to human toxicology but have not been well-studied in human breast cancer models [28].

Our findings indicate that PFOA exposure results in distinct response patterns in the OCT-based intracellular metrics, M and α. Although previous studies discussed above have established connections between the OCT-based intracellular metrics and cellular changes induced by various agents (such as formalin-fixation, microtubule inhibitors, Doxorubicin, *etc.*), the specific mechanisms of how PFOA, and potentially other PFAS, alters these metrics remain less understood. PFOA exposure has been linked to the induction of apoptosis and oxidative stress, including increased production of reactive oxygen species (ROS) and activation of apoptotic pathways, leading to cell damage and motility changes. Specifically, in breast epithelial cells such as MCF-10A, PFOA exposure results in mitochondrial membrane depolarization, DNA oxidation, and S-phase cell cycle arrest, ultimately leading to apoptosis [3,29]. Furthermore, PFOA exposure affects cell cycle regulation proteins (e.g., cyclin D, CDK4/6, p21/27/53), resulting in cell cycle arrest, inhibition of cell proliferation, and induction of apoptosis and necrosis [3,30].

Based on these findings, the reduction in cell viability and changes in intracellular motility metrics (decreased M and increased α) observed in PFOA-exposed MCF10DCIS.com spheroids might be associated with a combination of increased apoptosis, oxidative stress, and disruption of critical cellular processes. These mechanisms may collectively lead to impaired cell function and altered intracellular dynamics. Further experiments are needed to better understand the specific contributions of the different components (such as mitochondria, microtubules, *etc.*) to the changes in M and α.

Future studies may target PFAS-induced 3D MEC spheroid model response comparisons between these OCT metrics and standard assays such as MTT, while also potentially incorporating the measurement of S-phase fraction (SPF) to specifically assess the potential for increased cancer susceptibility. We also envision that the OCT-based metrics can serve as a novel biomarker for non-invasively detecting PFAS exposure, suggesting a promising direction for future screening applications. To establish this biomarker with greater fidelity, additional studies involving varied concentrations, different cell lines, extended time points, and more robust statistical analyses are necessary.

4. Conclusion

In this work, we investigated PFOA exposure-response in 3D MEC spheroid models using dynamic OCT, a non-invasive, longitudinal and high-throughput imaging modality, to assess the morphology and intracellular motility simultaneously. Despite no significant differences in volume and asphericity of the spheroids versus concentration, we observed internal structural alterations within the spheroids exposed to high PFOA concentration which appeared as small (~20 μm) holes, distinct from lumen formation, but similarly suggestive of regions of cell death. To study MEC motility responses to PFOA, two complementary OCT motility metrics were extracted from dynamic OCT: the inverse power law exponent, α, of the speckle fluctuation spectrum, and the autocorrelation-based motility amplitude, M, of the speckle intensity. The results revealed time- and concentration-dependent responses of MEC spheroid motility to the PFOA compound. Statistically significant differences between exposed cultures and their controls were attributed to cell death caused by exposure to a high concentration of PFOA.

Specifically, our linear regression model indicates that both PFOA concentration and culture time are highly significant predictors for both α and M ($p<0.001$ for all). Both PFOA concentration and culture time have positive associations with α and negative association with M, where increased

Biomedical Optics EXPRESS

α indicates suppression of higher frequency fluctuations (~> 2 Hz) relative to those at lower frequencies, and decreased M indicates overall suppression of intracellular motility. The multiple R^2 values for α and M are 0.334 and 0.729, respectively. This suggests that while our model captures the overall trends, there are limitations due to the absence of measurements between 1 and 4 days of culture time and between 100 µM and 500 µM of PFOA concentration levels. Further studies are necessary to examine more precise time points and concentration levels where significant changes occur. Our findings suggest that dynamic OCT can serve as a high-throughput device for screening environmental toxicants like PFAS. The intracellular motility metrics α and M can be used as biomarkers for assessing the impact of PFAS exposure on cellular health.

These findings establish the use of intracellular motility as a future biomarker of PFAS exposure as well as a starting point for future investigations into PFAS exposure-response of 3D organotypic models of the mammary gland. Future work will focus on refining this model by including additional concentrations (especially between 100 µM and 500 µM), time points (especially between Day 1 and 4), and cell lines, and by comparing the OCT metrics (M, α) with standard toxicological assays. This approach could be particularly valuable for rapid screening and prioritizing PFAS compounds. It also highlights the potential of dynamic OCT for high throughput and longitudinal studies of morphological structure and cell function in 3D organotypic models, with applications toward screening and prioritizing PFAS compounds.

Funding. National Institutes of Health (R01 ES 032730); National Science Foundation (CBET 180830).

Disclosures. The authors declare no conflicts of interest.

Data availability. Data underlying some of the results in this paper are available in Fig. S1 to S4 of Supplement 1. Underlying, raw image data are not publicly available at this time but may be obtained from the authors upon reasonable request.

Supplemental document. See Supplement 1 and Visualization 1 for supporting content.

References

1. E. M. Bell, S. De Guise, H. McCutcheon, *et al.*, "Exposure, health effects, sensing, and remediation of the emerging PFAS contaminants – Scientific challenges and potential research directions," Sci. Total Environ. **780**, 146399 (2021).
2. H. Jiang, H. Liu, H Liu, *et al.*, "Associations between polyfluoroalkyl substances exposure and breast cancer: a meta-analysis," Toxics **10**(6), 318 (2022).
3. P. Pierozan, F. Jerneren, and O Karlsson, "Perfluorooctanoic acid (PFOA) exposure promotes proliferation, migration and invasion potential in human breast epithelial cells," Arch. Toxicol. **92**(5), 1729–1739 (2018).
4. P. Pierozan, D. Cattani, and O Karlsson, "Perfluorooctane sulfonate (PFOS) and perfluorooctanoic acid (PFOA) induce epigenetic alterations and promote human breast cell carcinogenesis in vitro," Arch. Toxicol. **94**(11), 3893–3906 (2020).
5. S. Sun, H. Guo, J Wang, *et al.*, "Hepatotoxicity of perfluorooctanoic acid and two emerging alternatives based on a 3D spheroid model," Environ. Pollut. **246**, 955–962 (2019).
6. M. Forsthuber, R. Widhalm, C. Granitzer, *et al.*, "Perfluorooctane sulfonic acid (PFOS) inhibits vessel formation in a human 3D co-culture angiogenesis model (NCFs/HUVECs)," Environ. Pollut. **293**, 118543 (2022).
7. H. Wang, T. Xu, and D Yin, "Emerging trends in the methodology of environmental toxicology: 3D cell culture and its applications," Sci. Total Environ. **857**, 159501 (2023).
8. CD Paul, P Mistriotis, and K Konstantopoulos, "Cancer cell motility: lessons from migration in confined spaces," Nat. Rev. Cancer **17**(2), 131–140 (2017).
9. N. Kramera, A. Walzla, H Ungera, *et al.*, "In vitro cell migration and invasion assays," Mutation Research/Reviews in Mutation Research **752**(1), 10–24 (2013).
10. P. Pierozan, M. Kosnik, and O Karlsson, "High-content analysis shows synergistic effects of low perfluorooctanoic acid (PFOS) and perfluorooctane sulfonic acid (PFOA) mixture concentrations on human breast epithelial cell carcinogenesis," Environ. Int. **172**, 107746 (2023).
11. D. Huang, E. A. Swanson, J. G Lin, *et al.*, "Optical coherence tomography," Science **254**(5035), 1178–1181 (1991).
12. R. K. Chhetri, Z. F. Phillips, A. L Troester, *et al.*, "Longitudinal study of mammary epithelial and fibroblast co-cultures using optical coherence tomography reveals morphological hallmarks of pre-malignancy," PLoS One **7**(11), e49148 (2012).
13. K. Jeong, J. J. Turek, and D. D Nolte, "Speckle fluctuation spectroscopy of intracellular motion in living tissue using coherence-domain digital holography," J. Biomed. Opt. **15**(3), 030514 (2010).
14. D. D. Nolte, R. An, K Turek, *et al.*, "Holographic tissue dynamics spectroscopy," J. Biomed. Opt. **16**(8), 087004 (2011).

Biomedical Optics EXPRESS

15. P. Yu, L. Peng, D. D Mustata, *et al.*, "Time-dependent speckle in holographic optical coherence imaging and the health of tumor tissue," Opt. Lett. **29**(1), 68–70 (2004).
16. A. L. Oldenburg, R. K. Chhetri, J. B Cooper, *et al.*, "Motility-, autocorrelation-, and polarization-sensitive optical coherence tomography discriminates cells and gold nanorods within 3D tissue cultures," Opt. Lett. **38**(15), 2923–2926 (2013).
17. T. Kohlfaerber, M. Pieper, H Münter, *et al.*, "Dynamic microscopic optical coherence tomography to visualize the morphological and functional micro-anatomy of the airways," Biomed. Opt. Express **13**(6), 3211–3223 (2022).
18. C. Apelian, F. Harms, A. C Thouvenin, *et al.*, "Dynamic full field optical coherence tomography: subcellular metabolic contrast revealed in tissues by interferometric signals temporal analysis," Biomed. Opt. Express **7**(4), 1511–1524 (2016).
19. I. A. El-Sadek, A. Miyazawa, Y Shen, *et al.*, "Three-dimensional dynamics optical coherence tomography for tumor spheroid evaluation," Biomed. Opt. Express **12**(11), 6844–6863 (2021).
20. J. C. McIntosh, L. Yang, A. L Wang, *et al.*, "Tracking the invasion of breast cancer cells in paper-based 3D cultures by OCT motility analysis," Biomed. Opt. Express **11**(6), 3181–3194 (2020).
21. A. L. Oldenburg, X. Yu, M Gilliss, *et al.*, "Inverse power-law behavior of cellular motility reveals stromal-epithelial interactions in 3D co-culture by OCT fluctuation spectroscopy," Optica **2**(10), 877–885 (2015).
22. X Yu, AM Fuller, AL Blackmon, *et al.*, "Quantification of the Effect of Toxicants on the Intracellular Kinetic Energy and Cross-Sectional Area of Mammary Epithelial Organoids by OCT Fluctuation Spectroscopy," Toxicol Sci. **162**(1), 234–240 (2018).
23. L. Yang, X. Yu, A. L Fuller, *et al.*, "Characterizing optical coherence tomography speckle fluctuation spectra of mammary organoids during suppression of intracellular motility," Quant Imaging Med Surg **10**(1), 76–85 (2020).
24. N. Barnabas and D Cohen, "Phenotypic and molecular characterization of MCF10DCIS and SUM breast cancer cell lines," International Journal of Breast Cancer **2014**, 1–16 (2013).
25. K. R. Johnson, J. L. Leight, and V. M Weaver, "Demystifying the effects of a three-dimensional microenvironment in tissue morphogenesis," Methods Cell Biol. **83**, 547–583 (2007).
26. G. M. Sinclair, S. M. Long, and O. A. H Jones, "What are the effects of PFAS exposure at environmentally relevant concentrations?" Chemosphere **258**, 127340 (2020).
27. T. V. Nguyen, P. N. Trang, and A Kumar, "Understanding PFAS toxicity through cell culture metabolomics: Current applications and future perspectives," Environ. Int. **186**, 108620 (2024).
28. K. Li, P. Gao, L. Q Xiang, *et al.*, "Molecular mechanisms of PFOA-induced toxicity in animals and humans: Implications for health risks," Environ. Int. **99**, 43–54 (2017).
29. F. Salehi, H. Behboudi, S. K Kavoosi, *et al.*, "Chitosan promotes ROS-mediated apoptosis and S phase cell cycle arrest in triple-negative breast cancer cells: Evidence for intercalative interaction with genomic DNA," RSC Adv. **7**(68), 43141–43150 (2017).
30. S. H. Kim, K. C. Choi, and Y. H Lee, "Antiproliferative effects of quercetin through cell cycle arrest and apoptosis in human breast cancer MDA-MB-453 cells," Arch. Pharm. Res. **31**(10), 1281–1285 (2008).